fermentation

MDPI

Article

Adapted Feeding Strategies Enable Efficient Growth and Lipid Accumulation Using Untreated Crude Glycerol in Transition Scale with *Cutaneotrichosporon oleaginosum* ATCC 20509

Kevin Edward Schulz [1,*], Paula Hegmann [1], Bastian Dreher [1], Marina Schreidl [1], Katrin Ochsenreither [2] and Anke Neumann [1,*]

[1] Institute of Process Engineering in Life Sciences 2: Electrobiotechnology, Karlsruhe Institute of Technology, Fritz-Haber-Weg 4, 76131 Karlsruhe, Germany
[2] Department of Applied Logistics and Polymer Sciences, Hochschule Kaiserslautern–University of Applied Sciences, Carl-Schurz-Str. 10–16, 66953 Pirmasens, Germany; katrin.ochsenreither@hs-kl.de
* Correspondence: kevin.schulz@kit.edu (K.E.S.); anke.neumann@kit.edu (A.N.)

Abstract

Yeasts such as *Cutaneotrichosporon oleaginosum* can convert low-value side streams into single-cell oils with fatty acid profiles comparable to vegetable oils. Crude glycerol (CG), a byproduct of biodiesel production, offers a cost-effective substrate, but its variable impurity load often causes strong growth inhibition. In this study, two untreated industrial CG batches were characterized and evaluated in 2.5 L and 19 L stirred-tank fermentations. Direct batch cultivation on CG resulted in no measurable growth, whereas an adapted stepwise feeding strategy effectively mitigated early inhibition and restored biomass formation, metabolic activity, and lipid accumulation. In 2.5 L cultivations, apparent growth rates up to 0.51 h^{-1} and volumetric productivities up to 0.22 g L^{-1} h^{-1} were achieved, with lipid contents of ~30% and oleate-dominated fatty acid profiles. Fatty acid profiles remained oleate-dominated (~53–55% C18:1). Transition-scale (19 L) repeated-batch fermentations confirmed process robustness across > 640 h of operation, during which lipid content (~30–36%) and fatty acid composition (oleate ~51–53%) remained stable despite pronounced substrate-batch variability and increasing nitrogen limitation. These results demonstrate that untreated CG can be reliably valorized for lipid production using scalable feeding strategies without prior detoxification. This closes a gap between laboratory-scale feasibility studies and process-oriented, multi-cycle operation on industrial-grade feedstocks, confirming that feeding-driven inhibition control can ensure robust performance without substrate purification.

Keywords: yeast; single-cell oil; repeated batch; raw glycerol; adapted feeding

Academic Editor: Konstantinos G. Kalogiannis

Received: 23 January 2026
Revised: 6 March 2026
Accepted: 13 March 2026
Published: 15 March 2026

1. Introduction

The progressive depletion of economically viable fossil fuel reserves, together with the steadily increasing global demand for fuels and platform chemicals, underscores the urgent need for sustainable alternatives to safeguard future living standards. Crude oil, the traditional feedstock for fuels and oleochemicals, is a finite resource, and its continued exploitation substantially contributes to greenhouse gas emissions, thereby revealing the inherent limitations of a linear economy. Consequently, innovative solutions that decouple industrial production from fossil resources while simultaneously minimizing environmental impacts are required.

Oleaginous microorganisms, including the unconventional yeast *Cutaneotrichosporon oleaginosum*, represent a promising alternative to fossil oil resources due to their ability to produce single-cell oils (SCOs) [1,2]. These microbial lipids can account for 20–85% of the cell dry mass and exhibit fatty acid compositions comparable to palm oil, rendering them suitable for applications in biofuels, lubricants, and oleochemicals [3–6]. In contrast to conventional oil crops, microbial lipid production is independent of climate and seasonality, does not require arable land, and allows for the utilization of a wide variety of carbon sources. This versatility positions SCOs as a key pillar of future bio-based industries [7,8]. Beyond energy applications, SCOs are gaining increasing relevance in nutraceutical, cosmetic, and environmentally acceptable lubricant markets, further expanding their commercial potential [9,10].

Despite these advantages, microbial lipid production remains economically constrained, largely due to the high costs associated with conventional carbon sources such as glucose. Crude glycerol (CG), the primary byproduct of biodiesel manufacturing, represents a promising low-cost alternative. During transesterification, it accounts for approximately 10% of biodiesel output and is characterized by low price and high energy density. However, CG typically contains inhibitory compounds, including methanol, soaps, and residual catalysts, which can adversely affect microbial growth and lipid biosynthesis [11]. Consequently, avoiding costly purification or detoxification steps is crucial to ensure overall economic viability. Typical CG purification approaches include methanol removal by evaporation or distillation, acidification to split soaps into free fatty acids and salts, ion-exchange or adsorption for catalyst and salt removal, and membrane- or solvent-based separation techniques; however, these steps substantially increase process complexity, capital expenditure, and operating costs, limiting their applicability for low-value bulk bioprocesses [12,13].

Global biodiesel output reached ~52 million tonnes in 2022, with the EU (~13.7 Mt), USA (~10.2 Mt, primarily soybean oil), and Indonesia (~9.7 Mt, palm oil) representing the largest contributors. As a consequence, soybean-, palm-, and animal-fat-derived biodiesel streams represent the major industrial origins of CG worldwide [14–16]. The rapid expansion of biodiesel manufacturing has created a structural surplus of CG as a major by-product of transesterification processes. The continued growth of the biodiesel industry has therefore resulted in large quantities of CG entering the global market. This persistent oversupply has substantially reduced its market value and stimulated increasing interest in alternative valorization routes, including microbial conversion processes. Economically, CG is considerably cheaper than conventional carbon sources such as glucose or sucrose. Historically, CG has been reported to trade at around 100 USD t^{-1} (≈\$0.05 lb^{-1}), making it an attractive substrate for large-scale bioprocesses [17,18]. Beyond economics, glycerol's biochemical properties make it an excellent substrate for lipid-accumulating yeasts. Glycerol is highly reduced; its catabolism generates more NADH per carbon than glucose, providing enhanced reducing power for lipid biosynthesis and offering a thermodynamic advantage for anabolic processes such as fatty acid and triacylglycerol synthesis [19]. Although the efficiency of glycerol assimilation varies markedly among yeast species, the underlying metabolic framework is broadly shared. According to Klein et al. (2017) [20], most current knowledge on glycerol uptake and catabolism stems from studies with laboratory strains of *Saccharomyces cerevisiae*, in which glycerol is funneled into central carbon metabolism through well-established enzymatic routes. These studies demonstrate that glycerol is converted through pathways that ultimately produce dihydroxyacetone phosphate, thereby linking glycerol assimilation directly to glycolysis and energy metabolism. While substantial diversity exists in the ability of different yeasts to grow on glycerol, the fundamental organization of these pathways is conserved across fungi, and the review

highlights that the gene products required for glycerol utilization are well documented in *S. cerevisiae*. However, the authors also emphasize that knowledge regarding glycerol uptake and metabolism in non-*Saccharomyces* yeasts remains fragmentary, underscoring the need for further research on species that display superior growth on glycerol compared to conventional laboratory strains [20].

While several studies have demonstrated the feasibility of valorizing CG for microbial lipid production, important conceptual and methodological differences distinguish the present work from previous approaches. For example, a recent study utilizing *Rhodotorula glutinis* R4 investigated the combined valorization of sugarcane vinasse and CG within an integrated biorefinery framework, primarily aiming to couple biodiesel and bioethanol side streams to improve overall system sustainability [21]. That work focused on substrate co-utilization, nutrient supplementation via vinasse, and proof-of-concept lipid production under laboratory-scale batch conditions, with an emphasis on waste stream integration rather than on fermentation robustness or scalability.

Similarly, the study by Ram et al. on *Yarrowia lipolytica* SKY7 evaluated the effects of CG matrix composition and municipal wastewater sludge concentration on SCO production, highlighting the influence of substrate heterogeneity and co-substrate interactions on lipid accumulation [22]. This approach primarily addressed substrate quality effects and environmental biotechnological aspects at a small scale, rather than sustained process performance under industrially relevant fermentation conditions. In contrast, the present study focuses on CG as the sole carbon source, without co-substrate supplementation or detoxification, to reflect realistic industrial feedstock quality. By conducting transition-scale repeated-batch fermentations, the work emphasizes process scalability and stability, lipid accumulation dynamics, and biomass composition over multiple production cycles under representative hydrodynamic and feeding conditions. This process- and scale-oriented perspective provides novel insights into the robustness, scalability, and economic relevance of CG-based SCO production, thereby directly addressing the gap between laboratory-scale waste valorization studies and industrial bioprocess implementation. Prior reports have shown that feeding can offset crude-glycerol-related lag phases in various oleaginous yeasts, and two-stage or rate-controlled schemes can enhance oil titers [23–25]. However, most studies operated at a small scale, with pretreated substrates, or with different organisms. In contrast, our work employs untreated and non-sterilized industrial CG as the sole carbon source at transition scale (19 L) across more than 640 h of repeated-batch operation. A deliberately simple staged-feeding design was chosen to limit the inhibitor-to-biomass ratio during early growth, thereby restoring metabolism and lipid formation without substrate detoxification. We further show that lipid content and fatty acid composition remain robust despite substrate-batch variability, a requirement for biodiesel and oleochemical use.

2. Materials and Methods

If not stated otherwise, all chemicals were obtained from Carl Roth GmbH & Co. KG (Karlsruhe, Germany). Two different batches of CG, referred to as crude glycerol 1 (CG 1) and crude glycerol 2 (CG 2), were used in this study and were received as "untreated" crude glycerol from BRAIN Biotech AG (CG 1, Zwingenberg, Germany) and Hydroxy Energy GmbH (CG 2, Ochsenfurt, Germany). No further specification was received. CG batches were stored at room temperature in the dark and homogenized by thorough mixing prior to use. CG was used without further purification or sterilization and was added directly to the cultivation medium.

Due to the limited availability of industrial CG batches, all bioreactor fermentations were performed as single biological runs per condition. This constraint is explicitly acknowledged, and the study therefore focuses on robustness of operational trends, consistency

across scales, and reproducibility of physiological patterns rather than statistical hypothesis testing. Unless stated otherwise, all solutions and media were prepared using deionized water (conductivity < 1 μS cm^{-1}) produced using an in-house purification system. Inlet air was supplied via sterile filters prior to entering the bioreactors.

For 2.5 L scale fermentations, liquid media and heat-stable solutions were sterilized by autoclaving at 121 °C for 20 min. Heat-labile components, including trace element solutions, were sterilized by filtration through 0.2 μm pore-size membrane filters prior to use. The 19 L fermentation system was sterilized in situ by steam sterilization at 121 °C for 20 min.

2.1. Characterization of Crude Glycerol

Preliminary characterization of the CG batches was performed, including determination of ammonium, protein, carbohydrate, lipid, total carbon, and total nitrogen content, as described in Section 2.5 Analytics. Additionally, optical density at 600 nm was measured (see Section 2.6.9). Glycerol concentration was analyzed using HPLC (see Section 2.6.6).

2.2. Heuristic Simulation of Inhibitory Effects

For conceptual illustration and qualitative assessment of inhibitory effects during CG fermentation, a highly simplified heuristic simulation was implemented. The model was not intended to represent a quantitative kinetic description but to illustrate relative trends in inhibitor accumulation in relation to biomass development.

All variables were treated as relative, dimensionless quantities. Time represents discrete cultivation stages rather than continuous time. Inhibitory compounds in CG fermentation are defined as substances originating from biodiesel production or introduced during processing that negatively affect microbial growth and lipid synthesis. These include methanol, soaps (fatty acid salts), catalyst residues such as sodium or potassium hydroxide, and other trace impurities [13]. For the simulation, all inhibitory compounds were treated as a single aggregated factor rather than modeled individually. It was assumed that their effect on growth is proportional to their concentration in the fermentation broth and that these compounds are non-degradable under the applied process conditions. Each addition of CG was considered to introduce a fixed amount of inhibitors, which accumulate linearly over time with feeding events. No chemical or biological detoxification was assumed. The relative inhibition factor was defined as the ratio of inhibitor concentration to the biomass-related variable. Experimental validation was not performed through direct quantification of individual inhibitors; instead, the simulation was qualitatively compared to observed growth trends in bioreactor experiments. Growth delays and reduced biomass formation at higher CG concentrations were interpreted as indirect indicators of inhibitory effects. The simulation was implemented as a discrete step model, with inhibitor input occurring only at defined substrate feeding events.

Assumed exponential biomass increase was modeled using Equation (1):

$$B(t) = B_0 e^{(\mu t)} \quad (1)$$

where

- $B(t)$: Relative biomass-related variable at time t
- B_0: Initial value of the biomass-related variable
- μ: Specific growth rate parameter

Abstract dilution term with compound addition:

$$V(t) = V_0 + T(t) \quad (2)$$

where

- $V(t)$: Abstract dilution term.
- V_0: Initial reference value.
- $T(t)$: Cumulative inhibitor-related input.

In this context, $T(t)$ represents a cumulative relative input associated with CG addition rather than a physical quantity, and $V(t)$ is treated as an abstract dilution term without physical units.

Inhibitor accumulation:

$$T(t) = \Sigma\, a(t) \tag{3}$$

where

- $a(t)$: Relative inhibitor input associated with a feeding step.

Inhibitor-related concentration:

$$C(t) = T(t)/V(t) \tag{4}$$

Relative inhibition index:

$$R(t) = C(t)/B(t) \tag{5}$$

This simulation is intended solely as a qualitative conceptual illustration and not as a calibrated or predictive kinetic model.

2.3. Microorganism, Reactivation of Stored Cultures and Precultures

The strain used was *Cutaneotrichosporon oleaginosum* ATCC 20509. Previously prepared cryostocks consisting of 150 µL pure glycerol and 850 µL of a 20 g/L yeast culture were stored at −80 °C. For reactivation, cryostocks were streaked onto YM agar plates (10 g/L glucose, 3 g/L yeast extract, 3 g/L malt extract, 5 g/L peptone, 15 g/L agar; pH 7) and incubated for seven days. A single colony from the reactivated plate was transferred to a preculture flask containing liquid cultivation medium using a sterile inoculation loop. Precultures were performed in 250 mL baffled Erlenmeyer flasks with a working volume of 50 mL. The preculture medium corresponded to the nitrogen-limited bioreactor formulation and consisted of autoclaved nitrogen-limited mineral salt solution (8.99 g/L potassium dihydrogen phosphate, 0.12 g/L disodium hydrogen phosphate, 0.1 g/L sodium citrate dihydrate, 0.1 g/L yeast extract, 0.2 g/L magnesium sulfate heptahydrate, and 4.72 g/L ammonium sulfate) supplemented with 7.7% (*v*/*v*) sterile-filtered trace element solution (4 g/L calcium chloride dihydrate, 0.55 g/L iron(II) sulfate dihydrate, 0.475 g/L citric acid, 0.1 g/L zinc sulfate heptahydrate, 0.075 g/L manganese(II) sulfate monohydrate, and 100 µL/L sulfuric acid, 96%), 7.7% (*v*/*v*) autoclaved salt solution (10 g/L yeast extract and 20 g/L magnesium sulfate heptahydrate), and 7.7% (*v*/*v*) autoclaved glucose solution. Precultures were incubated for four days at 20 °C and 130 rpm. Subsequently, 1 mL of the first preculture was transferred to a second flask containing fresh medium, followed by an additional four-day incubation under identical conditions.

2.4. Stirred Tank Fermentations

Fermentations were carried out under nitrogen-limited conditions using the mineral salt medium described in 2.3, based on the formulation described by Gorte et al. [26]. The medium adjusted to pH 4 with 4 M phosphoric acid and 4 M sodium hydroxide consisted of four components: (i) a mineral salt solution; (ii) 2% (*v*/*v*) sterile-filtered trace element solution; (iii) 2% (*v*/*v*) autoclaved salt solution; and (iv) a carbon source adapted to the respective experimental setup further described below.

If not stated otherwise, fermentations were conducted for 144 h in 2.5 L Minifors bioreactor systems (INFORS HT, Bottmingen, Switzerland) with two Rushton turbines (INFORS HT, Bottmingen, Switzerland) controlled by Iris NT software (version 5.34.807.0997) with a working volume of 1.2 L. Cultivation parameters were selected based on the optimized conditions for *Saitozyma podzolica* DSM 27192 reported by Gorte et al. (2020) [26]: 22.5 °C, pH 4.0, agitation at 600 rpm, and aeration at 1 vvm. pH was monitored using an EasyFerm Plus PHI K8 225 probe (Hamilton Company, Reno, Nevada, USA), and dissolved oxygen tension (pO_2) was measured with a VisiFerm DO Arc 225 H0 probe (Hamilton Company, Reno, NA, USA). Exhaust gas composition was analyzed using freshly calibrated BlueVary sensors (BlueSens gas sensor GmbH, Herten, Germany), with data acquisition via BlueVis software (version 4.64.96). Automated pH control was achieved by addition of 4 M phosphoric acid and 4 M sodium hydroxide.

Inoculation volumes were calculated to achieve an initial optical density at 600 nm (OD_{600}) of 1.0, measured with a GENESYS 30 spectrophotometer (Thermo Fisher Scientific, Waltham, MA, USA). Foaming was controlled by daily addition of 100 µL Contraspum A 4050 (Zschimmer & Schwarz, Lahnstein, Germany) during the first 72 h, with dosage adjusted according to strain-specific requirements. Additionally, 24 mL of trace element solution and 24 mL of salt solution were fed daily during the first 72 h. Sampling was performed every 24 h, consisting of 5 mL for OD_{600} measurement and 20 mL for biomass and supernatant analysis. The 20 mL sample was centrifuged at 4700 rpm for 15 min; the supernatant was transferred to a 50 mL tube and stored at −20 °C, while the pellet was freeze-dried using a DW-10N freeze-dryer (Drawell Scientific Instrument Co., Ltd., Chongqing, China) for at least 72 h at −50 °C and 0.35 mbar before storage at −20 °C. All samples were preserved at −20 °C for subsequent analysis.

Three experimental setups were investigated. In the reference setup, pure glycerol was used as the sole carbon source at a concentration of 7.5% (v/v). In the second setup, pure glycerol was replaced by CG at the same concentration to assess the effects of impurities and compositional variability associated with industrial side streams. In the third setup, CG was supplied using an adapted feeding strategy while maintaining the same total substrate load of 7.5% (v/v). In this setup, untreated CG was added cumulatively, amounting to 9 mL after 24 h, 18 mL after 48 h, 27 mL after 72 h, and 36 mL after 96 h, with no further substrate addition thereafter.

2.5. Transition-Scale Fermentation

The scale-up from 2.5 L to 19 L was based on maintaining comparable oxygen-transfer conditions rather than specific power input or volumetric mass transfer coefficients due to different geometric properties of the used stir tank reactors. To ensure engineering equivalence, identical impeller design (Rushton turbines), and DOT-controlled aeration (>30% DOT at all times) were applied as primary scale-up criteria. Agitation and aeration rates were dynamically adjusted to maintain these conditions. Transition-scale fermentations were conducted in a 19 L stainless-steel stirred-tank bioreactor (Bioengineering AG, Wald, Zurich, Switzerland) equipped with two Rushton turbines and sensors for pH, temperature, and dissolved oxygen tension (DOT) using a nitrogen-limited mineral salts medium combined with an adapted glycerol feeding strategy similar to 2.4 with adapted volumes of 112.5 mL, 225 mL, 337.5 mL and 450 mL, respectively. Transition-scale experiments were performed with an initial working volume of 15 L. Repeated-batch operations were performed by partial harvest and medium replenishment at defined time points, while maintaining the same mineral medium composition if not stated otherwise and feeding strategy as described for lab-scale fermentations. One initial batch fermentation and three repeated-batch fermentations were conducted, each with a duration of 160 h. While the

initial batch fermentation was conducted using CG 1 and was inoculated with 1% (*v*/*v*) inoculum, repeated batch 1 used an inoculum size of 5% (*v*/*v*). Repeated batch 2 was initiated with CG 2 with 5% (*v*/*v*) inoculum. Repeated batch 3 employed the same CG batch as repeated batch 2 but utilized 60% inoculum, reducing the mineral salt content in half due to volume constraints. Throughout all fermentations, pH was controlled at 4.0 by automated addition of 4 M phosphoric acid and 4 M sodium hydroxide. The temperature was maintained at 22.5 °C, sterile air was supplied for aeration, and both agitation speed and airflow rate were dynamically adjusted to meet oxygen demand >30% DOT, starting from the initial settings of 200 rpm and 1 vvm.

2.6. Analytics

2.6.1. Cell Dry Weight

Cell dry weight (CDW) was determined gravimetrically in triplicate for each sample. Pre-dried and pre-weighed 1.5 mL reaction tubes were filled with 1 mL of cultivation broth and centrifuged at 13,000 rpm for 10 min. The supernatant was retained for further analyses. The cell pellet was washed with deionized water and centrifuged again at 13,000 rpm for 10 min. After removing the remaining water, the pellet was dried at 60 °C for 24 h and weighed using a precision balance (ADB220, KERN & SOHN GmbH, Balingen, Germany).

2.6.2. Protein Analysis

Protein content was determined using the commercially available DC™ Protein Assay (Bio-Rad Laboratories, Inc., Laboratories, Inc., Hercules, CA, USA), based on the Lowry method [27]. Lyophilized bovine γ-globulin (Bio-Rad Laboratories, Inc., Laboratories, Inc., Hercules, CA, USA) served as the calibration standard. To prepare the working solution, 20 µL of Reagent S was added per mL of Reagent A, yielding Reagent A′. For the calibration curve, a dilution series of the γ-globulin standard was prepared in a 1:1 mixture of deionized water and 2 M sodium hydroxide, resulting in concentrations of 200 µg/mL, 400 µg/mL, 600 µg/mL, 800 µg/mL, 900 µg/mL, 1000 µg/mL, 1250 µg/mL, and 1500 µg/mL. Samples were prepared by hydrolyzing 10 mg of freeze-dried biomass in 1 mL of 1 M sodium hydroxide for 1 h at 95 °C using a Univortemp MT100/MT100-C Thermoshaker (Universal Labortechnik GmbH & Co. KG, Leipzig, Germany). For optical analysis, 5 µL of each standard or sample was pipetted into a 96-well microplate. Subsequently, 25 µL of Reagent A′ and 200 µL of Reagent B were added, and the plate was shaken for 5 s in a Tecan Infinite® 200 PRO (Tecan Trading AG, Männedorf, Switzerland). Absorbance was measured at 750 nm after 15 min of incubation at room temperature. Photometric measurements were performed with standards in duplicate and samples in triplicate on each plate. Protein concentrations were calculated based on the standard curve and applied dilutions.

2.6.3. Carbohydrate Analysis

Carbohydrate content was quantified using the Anthrone–sulfuric acid assay [28]. Glucose stock solutions of 10 g/L and 5 g/L were prepared. The 10 g/L solution was diluted to 1:100, 1:200, and 1:500, while the 5 g/L solution was diluted to 1:50, 1:100, 1:200, and 1:500. These dilutions served as standards and were processed in the same manner as the samples. The Anthrone reagent was freshly prepared by dissolving 0.75% (*w*/*v*) Anthrone in 95% sulfuric acid and deionized water to obtain a final concentration of 0.1% (*w*/*v*). For sample preparation, 20 mg of freeze-dried biomass were weighed into 2 mL Safe-Lock tubes (Eppendorf SE, Hamburg, Germany), followed by the addition of 2 mL deionized water and thorough mixing. Dilutions of 1:20, 1:100, and 1:200 were prepared from each sample. For measurement, 100 µL of each sample or standard was transferred

into 2 mL Safe-Lock tubes, and 1 mL of ice-cooled Anthrone reagent was added. The mixture was homogenized by vortexing, kept on ice, and then incubated in a preheated Univortemp MT100/MT100-C Thermoshaker (Universal Labortechnik GmbH & Co. KG, Leipzig, Germany) at 800 rpm and 95 °C for 10 min. The reaction was stopped by placing the tubes on ice. Absorbance was measured in triplicate at 510 nm using a microplate reader, and carbohydrate concentrations were calculated based on the standard curve.

2.6.4. Fatty Acid Analysis

Lipid analysis of oleaginous yeast was performed via direct transesterification of biomass to fatty acid methyl esters (FAME) [29]. For transesterification, 30 mg of freeze-dried biomass were combined in glass test tubes with 1.5 mL n-hexane, 0.5 mL of heptadecanoic acid solution (2 mg/mL in hexane), and 2 mL of 15% sulfuric acid in methanol. The mixture was incubated in a Univortemp MT100/MT100-C Thermoshaker (Universal Labortechnik GmbH & Co. KG, Leipzig, Germany) at 100 °C and 1000 rpm for 2 h, with additional vortexing every 30 min to ensure thorough mixing. The reaction was stopped by cooling on ice. To improve phase separation, 1 mL of deionized water was added. Subsequently, 1 mL of the upper hexane phase containing FAME was transferred to an HPLC vial. Fatty acid profiles were analyzed qualitatively and quantitatively using gas chromatography (Agilent Technologies 6890 N Network GC System, Agilent Technologies, Santa Clara, CA, USA) equipped with a flame ionization detector (FID) operating at 1.9523 bar. Separation was achieved on an Agilent DB-Wax column (30 m × 0.25 mm). Two microliters of each sample were injected at an initial temperature of 160 °C. The oven temperature was increased from 160 °C to 240 °C at a rate of 2 °C/min and held at 240 °C for 15 min. A Marine Oil FAME Mix Standard (Restek Corporation, Bellefonte, PA, USA) was used for calibration and identification of FAME components.

2.6.5. Ammonium Analysis

To determine the ammonium concentration in the supernatant, the NH_4-N Spectroquant® test kit (Merck KGaA, Darmstadt, Germany) was employed in a downscaled format [30]. A calibration curve was prepared using ammonium sulfate dissolved in deionized water, with concentrations of 0 mg/L, 0.1 mg/L, 0.2 mg/L, 0.4 mg/L, 0.6 mg/L, 0.8 mg/L, 1.5 mg/L, 2 mg/L, 2.5 mg/L, 3 mg/L, 3.5 mg/L, and 4 mg/L. From each bioreactor sample and calibration standard, 250 µL were transferred into 1.5 mL reaction tubes. A micro-spoon of Reagent 2 from the kit was dissolved in 600 µL of Reagent 1 to prepare a combined reagent (Reagent 1 + 2). Subsequently, 30 µL of Reagent 1 + 2 were added to each tube, followed by thorough mixing. After a 5 min incubation, 5 µL of Reagent 3 were added to each tube. The samples were mixed again and incubated for an additional 5 min. Finally, 200 µL of each sample was transferred to a 96-well plate. Optical density at 690 nm was measured at room temperature using a Tecan Infinite® 200 PRO (Tecan Trading AG, Männedorf, Switzerland), and the ammonium concentration was calculated based on the calibration curve.

2.6.6. HPLC Analysis of Glycerin

Glycerol concentrations were determined using an Agilent 1100 Series high-performance liquid chromatography (HPLC) system equipped with an ion-exclusion Rezex ROA Organic Acid H^+ (8%) column (Phenomenex, Inc., Torrance, CA, USA). Separation was performed with a 10 µL injection volume at 50 °C, using a mobile phase of 5 mM sulfuric acid at a flow rate of 0.5 mL/min, and detection was achieved with a refractive index detector. Quantification was based on calibration curves prepared with glycerol concentrations ranging from 0.1 g/L to 10 g/L.

2.6.7. Total Carbon (TC) and Total Nitrogen (TN) Analysis

Total carbon (TC) content was measured using a TOC-VCPN analyzer (Shimadzu Corporation, Kyoto, Japan), and total nitrogen (TN) content was determined with a TNM-1 module (Shimadzu Corporation, Kyoto, Japan). The system operated with synthetic air containing 20.5% oxygen (Air Liquide, Paris, France) and an ASI SA24 autosampler (40 mL, Shimadzu). Air pressure was regulated to 200 kPa and 150 kPa via internal barometers. The combustion chamber temperature was set to 680 °C for TC analysis and 720 °C for TN analysis. Halogen gases generated during the process were removed using a halogen scrubber (model p/n 630-00992, Shimadzu Corporation, Kyoto, Japan). All analyses were managed through TOC-ControlV software, version 1.07.00 (Shimadzu Corporation, Kyoto, Japan). TC analysis was carried out with 2/3 injections, 2 washes, SD Max of 0.1000, CV Max of 2.00%, no acid addition with an injection volume of 50 µL, an expected concentration range of 767.5 and 4:50 min total integration time. TN analysis was carried out with 2/3 injections, 2 washes, SD Max of 0.1000, CV Max of 2.00%, no acid addition with an injection volume of 50 µL, an expected concentration range 250 and 4:50 min total integration time.

2.6.8. Gas Analytics

Calculations of gathered gas composition data were done similarly to Hartmann et al. [31]. The calculations for oxygen transfer rate (OTR), carbon transfer rate (CTR) and respiratory quotient (RQ) are shown in Equations (6)–(8).

$$OTR = \frac{p_{gas} F_{gas,in}}{R T_{gas}} \left(y_{O_2,in} - \frac{1 - y_{O_2,in} - y_{CO_2,in}}{1 - y_{O_2,off} - y_{CO_2,off}} y_{O_2,off} \right) \tag{6}$$

$$CTR = \frac{p_{gas} F_{gas,in}}{R T_{gas}} \left(y_{CO_2,off} \frac{1 - y_{O_2,in} - y_{CO_2,in}}{1 - y_{O_2,off} - y_{CO_2,off}} - y_{CO_2,in} \right) \tag{7}$$

$$RQ = \frac{CTR}{OTR} \tag{8}$$

2.6.9. Optical Density at 600 nm

Determination of optical density at 600 nm (OD_{600}) was conducted using a GENESYS 30 spectrophotometer (Thermo Fisher Scientific, Waltham, MA, USA). Optical density measurements were performed in 1 cm path-length transparent plastic cuvettes (BRAND GmbH + Co. KG, Wertheim, Germany).

2.6.10. Data Analysis

Data analysis and visualization were performed using Microsoft Excel and OriginPro Ver. 10.0.0.154. Excel was used for preliminary data processing, calculation of averages, and organization of experimental datasets. Graphical representation and advanced data evaluation were conducted in OriginPro Ver. 10.0.0.154. All analytical measurements (CDW, protein, carbohydrate, fatty acids, ammonium, glycerol) were performed in technical triplicate. Averages and standard deviations were calculated in Excel. Gas-analysis signals (OTR, CTR, RQ) were smoothed using LOWESS filtering in OriginPro Ver. 10.0.0.154 to reduce noise without imposing a kinetic model. Specific growth rates µ, volumetric productivities and substrate uptake rates were calculated from time-resolved concentration differences between sampling points. Gas-phase variables (*OTR*, *CTR*, *RQ*) were calculated according to Equations (6)–(8) in Section 2.6.8.

3. Results and Discussion

The following results are based on two untreated industrial CG batches. All fermentations were conducted as single biological runs (n = 1) due to the limited availability of industrial CG. This limitation is explicitly acknowledged, and results are interpreted as operational trends rather than statistically validated performance metrics, consistent with similar long-term CG studies relying on limited replication [17]. While CG 1 was used for the establishment of the feeding strategy in 2.5 L and as a reference in the 19 L scale fermentation, CG 2 was used to assess the general applicability of different CG batches and different inoculum sizes using the adapted feeding strategy.

Comprehensive compositional analysis of the two different CG batches revealed marked variability, most prominently in the carbon-to-nitrogen (C/N) ratio (Table 1). CG 1 exhibited an extremely high C/N (~2.0×10^4), whereas CG 2 showed a still very high but substantially lower value (~4.2×10^2). The observed compositional variability aligns with typical ranges reported for biodiesel-derived CG, which often exhibits strong fluctuations in glycerol purity, soap content, methanol residues, ash, and trace metals depending on the feedstock and catalyst system [14,17]. Such heterogeneity is characteristic of alkaline-catalyzed biodiesel processes and reflects upstream washing efficiency, methanol recovery, and catalyst selection, consistent with values reported for industrial CG streams in previous studies. Nitrogenous components were near or below detection, while protein and carbohydrate fractions were negligible, and the lipid fraction was <2% in CG 1 (Table 1). Given that nitrogenous components were at or below the detection limit, the calculated C/N ratios should be interpreted as indicative descriptors of substrate composition rather than biologically accessible C/N ratios. Such profiles are consistent with the well-documented heterogeneity of biodiesel-derived CG and reflect upstream differences in feedstock oil, alkaline catalysts (NaOH/KOH), methanol recovery, and subsequent neutralization and washing, which govern impurity carry-over (methanol, soaps/fatty acid salts, salts, ash, trace metals) and thereby the inhibitory burden during microbial conversion [13,14].

Table 1. General composition analysis of applied untreated non-sterilized crude glycerol (CG) batches received from industry. Protein content, carbohydrate content and lipid content were determined as percentual value while glycerol concentration is shown in g/L. The ammonium content of crude glycerol 2 (CG 2) was below the detection level of 0.01.

	Proteins/%	Carbohydrates/%	Lipids/%	Ammonium/g/L	C/N Ratio	OD_{600}	Glycerol Concentration/g/L
Crude glycerol 1	0.46	0.06	1.80	0.02 ± 0.02	20,357	0.235	620
Crude glycerol 2	0.02	0.35	n. d.	0.00 *	420	7.840	810

* Below the detection level of 0.01.

This variability matters bioprocess-wise: numerous studies show that CG impurities can slow down growth, shift metabolism (e.g., toward citric acid formation), or inhibit lipid accumulation, with ion content ($Na^+/K^+/SO_4^{2-}$) and residual soaps frequently implicated [13,32]. These observations are consistent with reports describing that methanol, fatty acid salts, and residual alkali exert their strongest inhibitory effects at low biomass concentrations, causing prolonged lag phases or complete growth arrest [17,33]. Untreated industrial CG contains methanol, soaps/fatty acid salts, residual alkaline catalysts (Na^+/K^+ hydroxides), ash, and other minor organics. These impurities can delay growth, trigger osmotic stress, alter pH, or shift carbon flux toward overflow products such as citric acid, with Na^+, K^+, and sulfate loads being particularly inhibitory to some yeasts.

Preliminary growth experiments indicated long lag phases on untreated CG, motivating a simple, qualitative inhibition model that relates an aggregated inhibitor input to biomass development (Section 2.2). While intentionally heuristic, the simulation shown in

Figure 1 depicts a key operational insight confirmed across the lipid-fermentation literature: the magnitude of inhibition is highest when biomass concentration is low; consequently, large initial crude-glycerol doses can fully suppress growth, as observed in our batch controls. Staged feeding avoids this by lowering the effective inhibitor-to-biomass ratio in the early phase. This mechanistic rationale is consistent with previous studies reporting that pulsed or rate-controlled feeding circumvented inhibition and restored lipid formation in fermentations with toxic carbon sources. Consequently, high initial CG supplementation is risky, whereas pulsed or continuous addition mitigates inhibition, an approach echoed in fed-batch studies where adapted feeding avoided CG-induced inhibition and restored lipid productivity [23,24].

For *C. oleaginosum* specifically, modeling and experimental work in the literature support efficient lipid accumulation on glycerol at elevated C/N ratios and indicate different process levers to sustain lipid synthesis, reinforcing the rationale to keep inhibitory pressure low while carbon source supply remains abundant, suitable for our heuristic model [34].

As baseline three conditions in 2.5 L scale only using CG 1 to establish the adapted feeding strategy were studied: (i) CG 1 (7.5% (*v*/*v*) initial concentration), (ii) pure glycerol (7.5% (*v*/*v*) initial concentration) and (iii) CG 1 with adapted stepwise feeding (cumulative 9, 18, 27, 36 mL at 24 h intervals to 72 h), keeping total substrate concentration identical.

While the CG 1 batch fermentation (i) is a reference to evaluate growth without an adapted feeding strategy, the batch fermentation on pure glycerol (ii) was conducted to study growth on glycerol in general. In both fed-batch fermentations, a feeding strategy based on the simulation in Figure 1 was applied. The cumulative pulses (9, 18, 27, and 36 mL at 24 h intervals) were applied as fixed feeding steps. These predefined pulse volumes ensured that the total crude-glycerol input matched the batch control while distributing the inhibitory load over time to maintain a lower inhibitor-to-biomass ratio during early growth. CG was added without sterilization or detoxification. Each pulse was supplied after the scheduled 24 h sampling. In the CG 1 batch fermentation, without adapted feeding, measurable growth or respiratory activity (Figures 2A and 3A) was not detected, consistent with inhibitors surpassing the tolerable per-biomass threshold. In contrast, adapted feeding resulted in growth (Figures 2C,D and 3C,D), ammonium consumption, and off-gas profiles (rise in CTR and OTR) resembling the glycerol cultivation (Figures 2B and 3B), indicating restored metabolic activity under CG despite impurities.

As shown in Table 2, adapted feeding substantially increased apparent growth and production performance, with μ_{Max} rising from 0.16 h^{-1} under batch cultivation on pure glycerol to approximately 0.5 h^{-1} under adapted feeding, and volumetric productivities (P_v) increasing from ~0.01 to ~0.21 g L^{-1} h^{-1}. While n = 1 precludes inference testing, the directional agreement across biomass, substrate, and gas analytics supports the operational value of incremental CG addition to overcome early-phase inhibition—in line with prior fed-batch reports where pulsed or low-rate feeds reduced lag and improved lipid titers on CG in other oleaginous yeasts [23,25].

Table 2. Key performance indicators μ_{Max}, $Y_{X/S}$ and P_v of fermentations in a 2.5 L scale. Maximum growth rates represent apparent values calculated from biomass data obtained at 24 h sampling intervals, reflecting averaged kinetics rather than instantaneous specific growth rates.

Cultivation	μ_{Max}/h^{-1}	$Y_{X/S}$ /$g_{biomass}$/$g_{Substrate}$	P_v/g·L^{-1}·h^{-1}
Crude glycerol 1	no growth	no growth	0.013
Pure glycerol	0.157	0.116	0.123
Adapted feeding 1	0.514	0.763	0.211
Adapted feeding 2	0.499	0.560	0.215

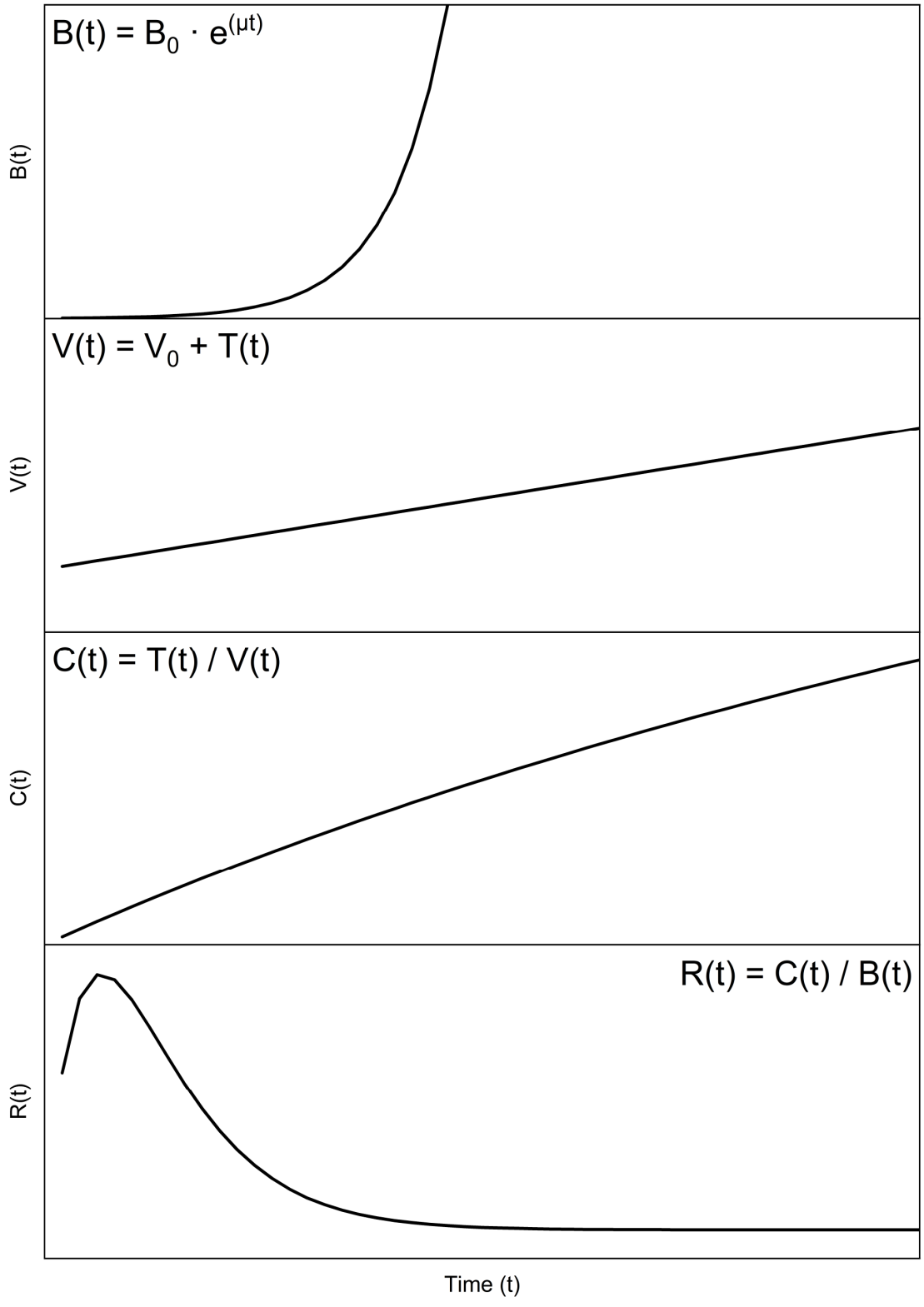

Figure 1. Simulated trends in time of relative biomass-related variable $B(t)$; the change in the abstract dilution term $V(t)$; the change in inhibitor-related concentration $C(t)$; and the behavior of relative inhibition index $R(t)$. All axes are displayed linearly. The conceptual illustration shown does not aim to predict kinetics but serves to visualize the qualitative dependency between initial biomass and effective inhibitor burden per cell. All used formulas are further explained in Section 2.

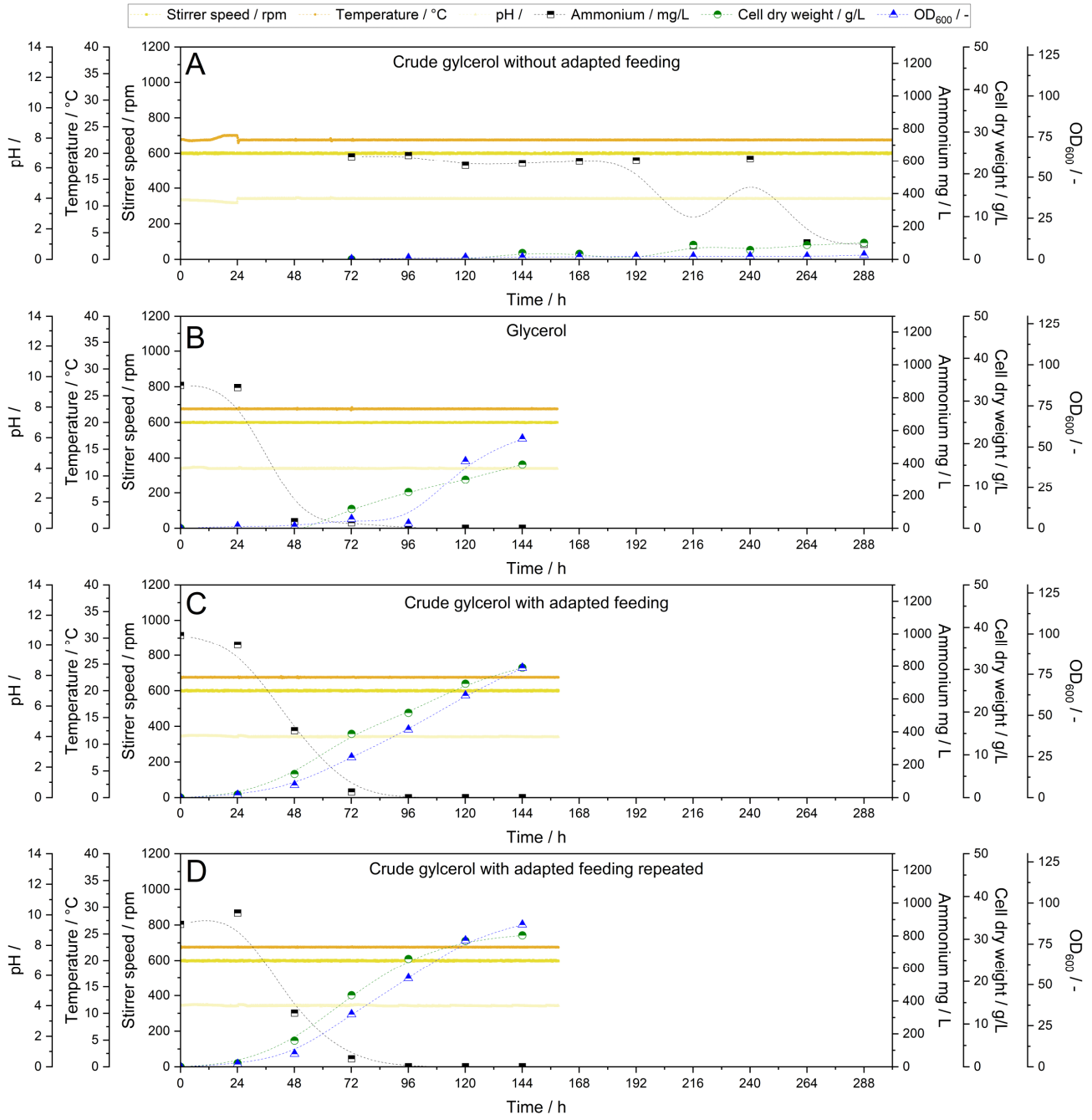

Figure 2. Cultivation parameters pH, temperature, stirrer speed, OD_{600}, cell dry weight and ammonium concentration of 2.5 L stirred tank fermentations of references with (**A**) CG without adapted feeding, (**B**) pure glycerol, and of (**C**,**D**) with CG with adapted feeding of the strain *C. oleaginosum*. CG 1 was used. Dotted lines were added only for visual orientation (n = 1).

For each fermentation, biomass was gathered at the endpoint of its respective cultivation and analyzed for biomass composition. The obtained composition data further support the beneficial effects of the adapted feeding strategy (Figure 4). Biomass from the CG 1 batch reference differed markedly in composition, showing reduced lipid content and carbohydrate fractions, and likely represents metabolically stressed cells derived from the inoculum. In contrast, in PG batch fermentation, biomass composition resembled a typical nitrogen-limited *C. oleaginosum* profile (proteins ~17%, carbohydrates ~25%, lipids ~31%). Adapted CG feeding resulted in a comparable lipid fraction (~30%), indicating that lipid

accumulation can proceed on untreated CG when inhibition is managed by an appropriate feeding regime.

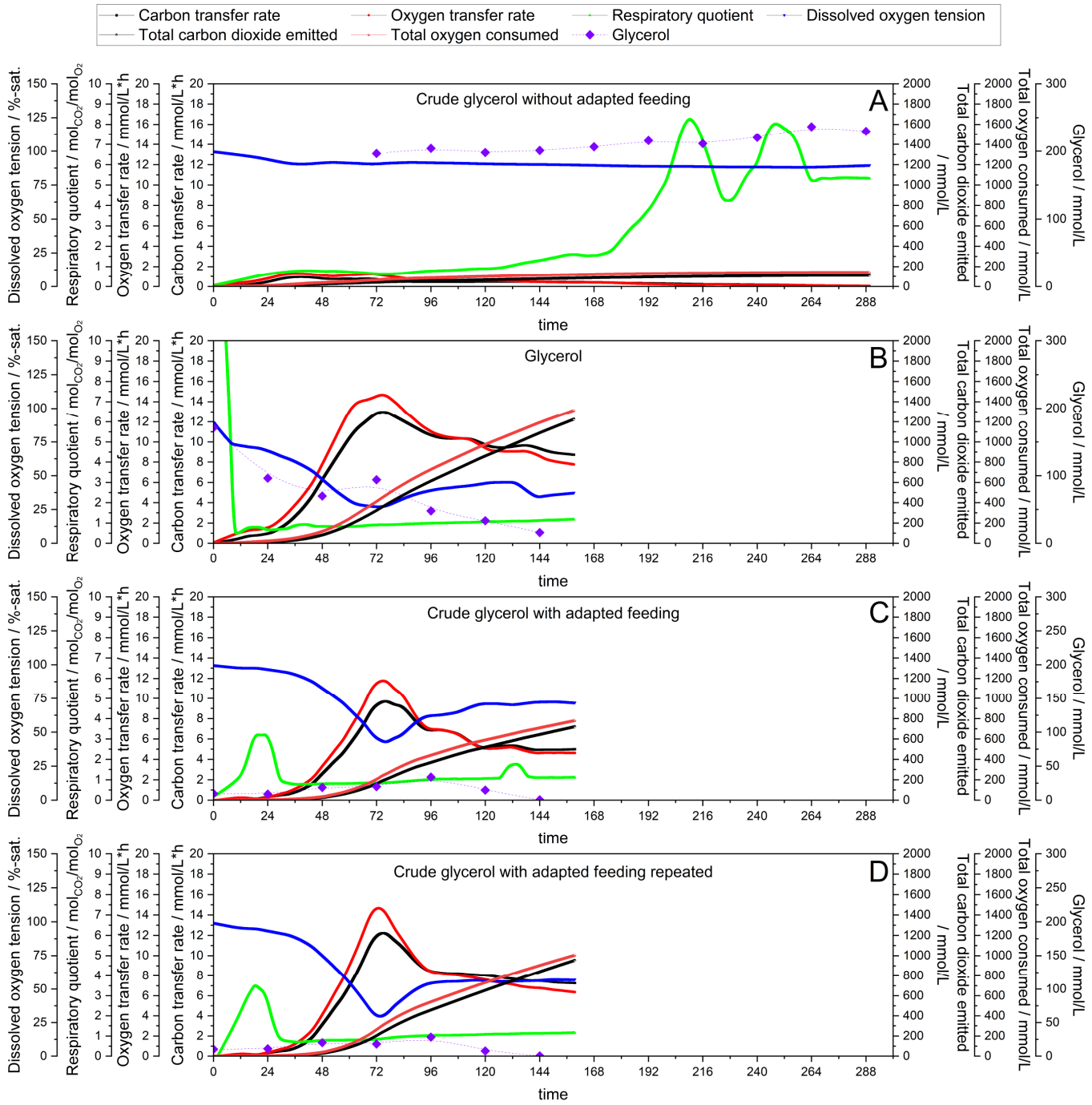

Figure 3. Gas analytics and glycerol concentration of 2.5 L stirred tank fermentations of references with (**A**) CG without adapted feeding, (**B**) pure glycerol, and of (**C**,**D**) with CG with adapted feeding of the strain *C. oleaginosum*. Crude glycerol 1 (CG 1) was used. The cumulative curves represent the total carbon dioxide emitted and the total oxygen consumed, which increase continuously over the course of the cultivation. In contrast, the carbon transfer rate and oxygen transfer rate are shown as peak-shaped profiles reflecting the instantaneous metabolic activity of the culture. Carbon dioxide–related parameters are shown in black, whereas oxygen-related parameters are shown in red. Dotted lines were added only for visual orientation (n = 1).

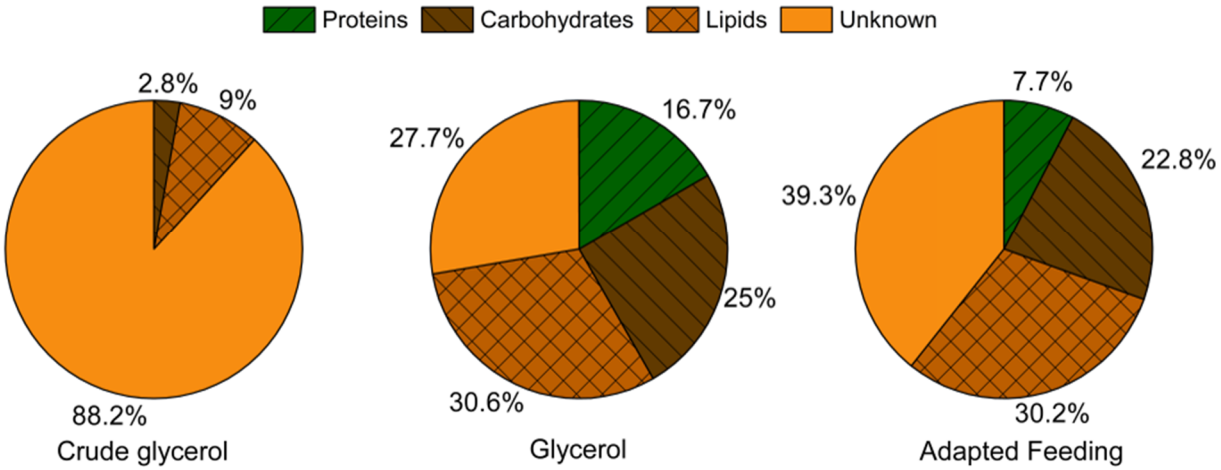

Figure 4. Relative endpoint biomass composition of 2.5 L stirred tank fermentations with *C. oleaginosum* after 144 h of fermentation time. For protein determination of the reference fermentation with CG not enough biomass was produced. The used CG batch was CG 1 (n = 1).

The reported lipid profile of oleaginous yeasts grown on glycerol is typically enriched in C18:1, C16:0, C18:2, and C18:0, which align with biodiesel and oleochemical specifications [35,36]. Differences in fatty acid profiles can be mechanistically explained by regulation of acetyl-CoA flux, NADPH availability, and desaturase activity. Nitrogen limitation typically favors oleate-rich profiles (C18:1), whereas metabolic stress or incomplete carbon assimilation increases polyunsaturated fractions such as linoleate (C18:2). These trends align with published FA shifts observed in glycerol-based fermentations [17,19]. The fatty acid (FA) profiles detailed in Figure 5 and Table S1 confirm a similar composition under adapted CG feeding in comparison to pure glycerol biomass (Figure 5): biomass from both PG and adapted-CG fermentations were dominated by oleate (~53–55%), with palmitate (~20–21%) and stearate (~10%) as major co-constituents—consistent with oleaginous yeast oils considered suitable for biodiesel due to cetane and oxidative stability contributions from monounsaturates [35,36]. By contrast, CG without adapted feeding (no growth) showed a stressed fatty acid profile with elevated linoleate fractions (>28%), consistent with starvation signatures rather than productive lipid biosynthesis. Further insights into the FA profile are provided in Figure 5; detailed numbers are available in the additional information in Table 1.

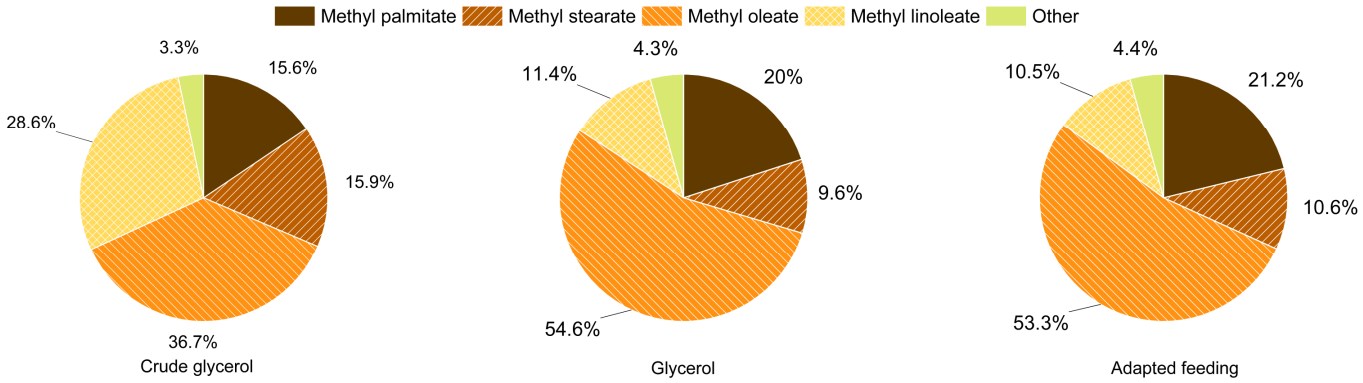

Figure 5. Fatty acid profile of endpoint biomass produced in 2.5 L stirred tank fermentations with *C. oleaginosum* using CG 1, pure glycerol and adapted feeding with CG 1 (n = 1).

Taken together, these results do not claim statistical equivalence (n = 1) but are consistent with findings from the related literature: for untreated CG, feed design is often sufficient to offset impurity-linked growth delays and to regain lipid titres and

quality—especially when glycerol is the sole carbon source and the process remains oxygen-sufficient [13,23].

The fermentation process was scaled up from a 2.5 L laboratory scale to a 19 L transition scale to improve process representativeness and to reduce scale-up risk. At a 2.5 L scale, key engineering parameters such as mixing efficiency, oxygen transfer, and foaming behavior can differ significantly from larger-scale systems, potentially limiting the predictability of downstream scale-up. In addition, repeated-batch fermentations were tested to evaluate process robustness.

At the 19 L transition scale, a repeated-batch regime with DOT-guided adapted aeration and agitation was implemented to address dynamic oxygen demand. Across the initial batch fermentation and three repeated batches, key process variables remained within defined operational ranges (stable pH and temperature; DOT maintained above the set threshold of 30%), and growth trends in OD_{600} and CDW were consistent with expected repeated-batch cultivation patterns (Figure 6).

At the transition scale, the initial batch fermentation achieved an apparent maximum growth rate of $\mu_{Max} = 1.56\ h^{-1}$ and a volumetric biomass productivity of $P_v = 0.15\ g{\cdot}L^{-1}{\cdot}h^{-1}$ (Table 3).

Table 3. Key performance indicators of *C. oleaginosum* fermentations in a transition scale. The reported μ values should be interpreted as operational performance indicators rather than physiological maximum growth rates, as their calculation is constrained by sampling resolution. CG 1 was used for the initial batch and repeated batch 1 and CG 2 for repeated batch 2 and repeated batch 3.

Cultivation	μ_{Max}/h^{-1}	$Y_{X/S}$ $/g_{biomass}/g_{Substrate}$	$P_v/g{\cdot}L^{-1}{\cdot}h^{-1}$
Initial batch	1.559	0.580	0.146
Repeated batch 1	0.870	0.527	0.092
Repeated batch 2	1.378	0.352	0.104
Repeated batch 3	0.597	0.146	0.057

Scale-up from 2.5 L to 19 L was successful: transition-scale operation delivered substantially higher apparent growth rates (μ_{max} up to 1.56 h^{-1} at 19 L vs. ~0.50 h^{-1} with adapted feeding at 2.5 L; Table 2) while maintaining volumetric productivities in the same order of magnitude (0.10–0.15 $g{\cdot}L^{-1}{\cdot}h^{-1}$ at 19 L vs. ~0.21 $g{\cdot}L^{-1}{\cdot}h^{-1}$ at 2.5 L). The increased growth kinetics at 19 L are consistent with reports that improved oxygen transfer, reduced mixing gradients, and higher cell densities promote more stable lipid synthesis pathways during glycerol conversion [17]. The preservation of FA composition across repeated batches agrees with studies describing the high robustness of oleaginous yeast lipid profiles at elevated cell densities and oxygen-sufficient conditions. This indicates that scale-up primarily enhanced kinetic behavior (faster growth) without compromising overall biomass formation efficiency. Consistent with this, process variables remained within defined operational ranges (pH and temperature stable; DOT above the control threshold of 30%), across more than 640 h of transition-scale repeated-batch operations (Figure 6), and fatty acid composition was preserved, with oleate consistently representing ~51–53% of total fatty acids. This robustness is notable given the pronounced compositional variability between CG batches and the stronger nitrogen limitation enforced in later cycles. Product-composition stability under these conditions is essential for downstream biodiesel and oleochemical applications. Reports on semi-continuous or continuous systems with cell recycle demonstrate similarly high operational robustness for oleaginous yeasts, suggesting that strategies that maintain high cell density can further stabilize long-term production.

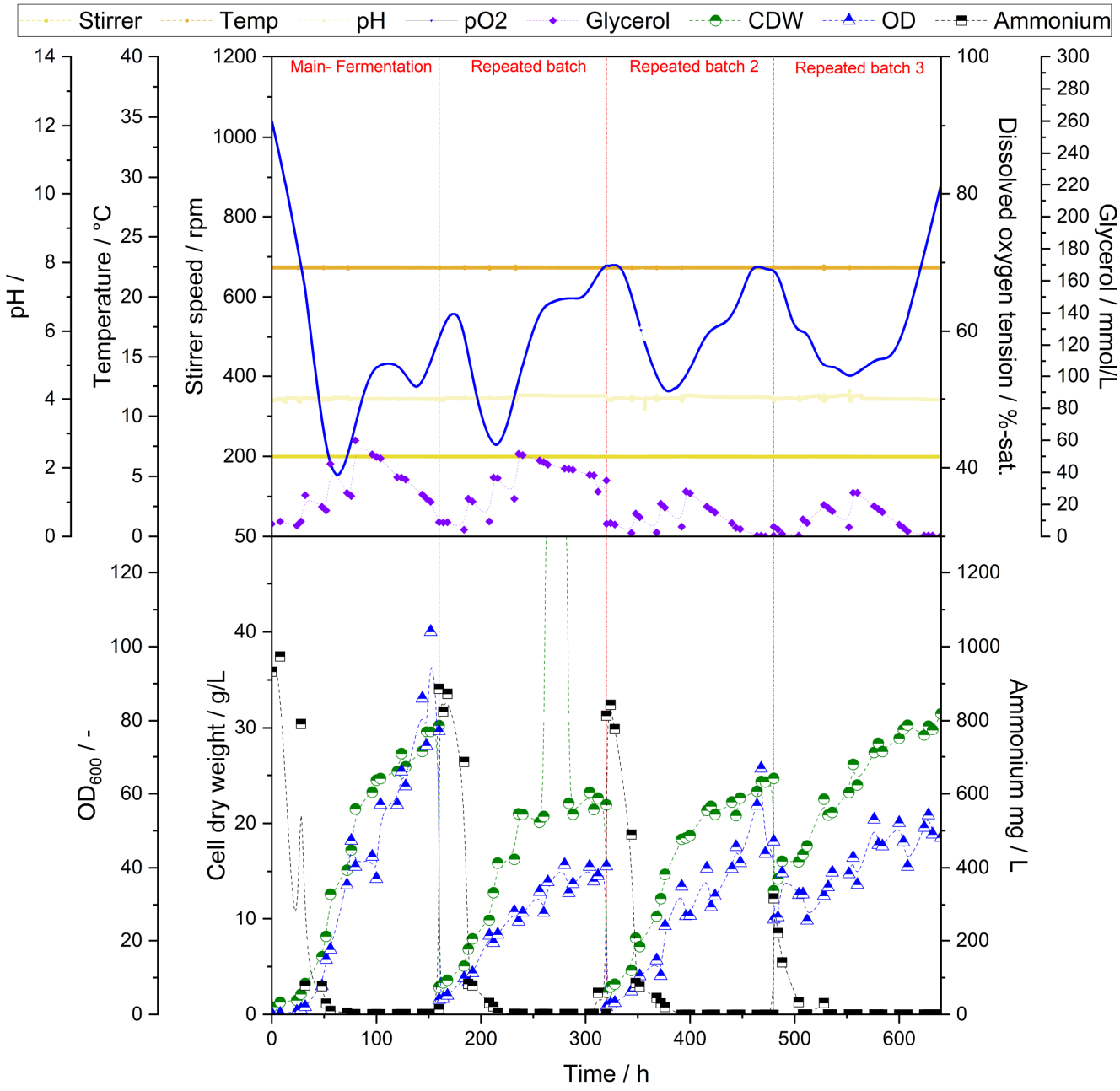

Figure 6. Cultivation parameters pH, temperature, stirrer speed, dissolved oxygen tension, glycerol concentration, cell dry weight, ammonium concentration and optical density at 600 nm of transition-scale fermentations with *C. oleaginosum* and separation in repeated batches. CG 1 was used for the initial batch and repeated batch 1 and CG 2 for repeated batch 2 and repeated batch 3. Dotted lines were added only for visual orientation (n = 1). Inoculum for initial fermentation was 1% (v/v), for repeated batch 1 and 2 it was 5% (v/v) and for repeated batch 3 it was 60% (v/v).

In subsequent repeated-batch fermentations, the effect of CG batch variability on process performance was evaluated at a constant inoculum size of 5% (v/v). As shown in Figure 6 and summarized in Table 3, the two untreated industrial glycerol batches exerted a pronounced influence on growth dynamics. Cultivation with CG 1 resulted in slower kinetics (μ_{Max} = 0.87 h^{-1}) and a lower volumetric productivity (P_v = 0.09 $g{\cdot}L^{-1}{\cdot}h^{-1}$), whereas the use of CG 2 under otherwise identical conditions accelerated growth (μ_{Max} = 1.38 h^{-1}) and increased productivity (P_v = 0.10–0.15 $g{\cdot}L^{-1}{\cdot}h^{-1}$). This indicates that at low inoculum levels, batch-specific differences in CG composition can substantially

modulate growth kinetics, likely due to differences in the effective inhibitor burden per unit biomass.

For repeated batch 3, a high inoculum level of 60% (v/v) was deliberately combined with a partial replacement of mineral medium, resulting in an approximately halved initial mineral salt and nitrogen availability. This design choice reflects a typical repeated-batch operation, where medium replenishment is only partial and nutrient carry-over from previous cycles cannot be avoided. Maintaining a high inoculum ensured a low inhibitor-to-biomass ratio and minimized lag phase effects, while the reduced nitrogen supply imposed a stricter nitrogen-limited regime representative of prolonged repeated-batch cultivation. This combination allowed the decoupling of early phase inhibition effects from nutrient-driven metabolic responses, enabling assessment of process robustness under increasingly nitrogen-limited conditions. Such conditions are known to favor lipid accumulation over biomass formation in oleaginous yeasts, while simultaneously reducing maximum growth rates. The applied setup, therefore, reflects an industrially relevant trade-off between sustained process continuity and nutrient limitation rather than an experimentally imposed stress scenario [36,37]. Within this deliberately imposed process regime, cultivation in repeated batch 3 resulted in reduced growth kinetics. KPI of the repeated-batch fermentations are summarized in Table 3.

Overall, the key performance indicators signify that transitioning from batch to repeated-batch operation leads to a gradual reduction in biomass yield, reflecting the increasing influence of nutrient carry-over and partial medium replacement. While high inoculum levels and adapted feeding strategies effectively govern early-phase growth kinetics and volumetric productivity by mitigating inhibition, progressively reduced mineral salt and nitrogen availability shift process control toward a stricter nitrogen-limited regime. Under these conditions, growth rates decline as metabolic flux is redirected from biomass formation toward maintenance and lipid storage (30% to 36% increase). CG batch variability further modulates growth kinetics once nitrogen becomes limiting, whereas lipid content and fatty acid composition remain robust across repeated batches. This demonstrates that the applied repeated-batch strategy primarily affects kinetic and yield-related parameters, while lipid quality is preserved despite variations in inoculum regime, nutrient availability, and CG source.

Changes in inoculum size were reflected in biomass composition, as shown in Figure 7. Fermentations with small inoculum sizes displayed an increased protein fraction and a reduced lipid share, which is indicative of prolonged growth and a delayed transition into lipid storage metabolism. In contrast, repeated batch 3 initiated with a 60% inoculum approached lipid content of approximately 36% of dry biomass. This modulation of biomass composition as a function of inoculum history and physiological state is consistent with previous findings from Duman-Ozdamar et al., showing that key process parameters—including C/N ratio, temperature, and feeding strategy—systematically steer lipid accumulation in *C. oleaginosum* and related oleaginous yeasts [36].

Despite these shifts in biomass composition, FA profiles remained stable across all repeated batches (Figure 8, Table S2). Detailed numbers are available in the additional information Table 2. Oleic acid consistently represented the dominant FA, accounting for approximately 51–53% of total FAs, irrespective of inoculum size or CG batch. This compositional stability indicates that repeated-batch operation and substrate variability did not lead to an adverse drift in lipid quality. Such robustness is characteristic of glycerol-based fermentations with oleaginous yeasts and is widely recognized as advantageous for biodiesel and oleochemical applications, where oleate-rich profiles are desirable due to their favorable physicochemical properties [35,36].

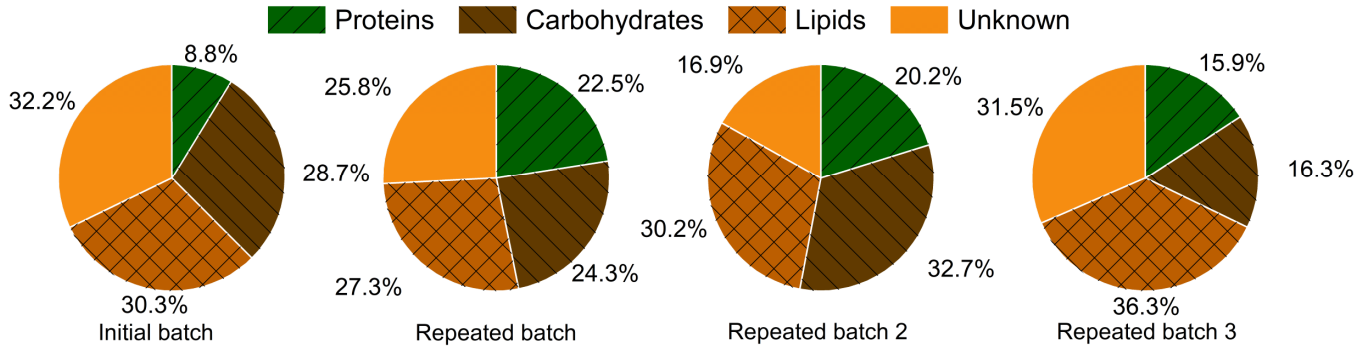

Figure 7. Endpoint biomass composition of the 19 L transition-scale fermentations with *C. oleaginosum*. CG 1 was used for the initial batch and repeated batch 1 and CG 2 was used for repeated batch 2 and repeated batch 3. Inoculum for initial fermentation was 1% (*v*/*v*), for repeated batch 1 and 2 it was 5% (*v*/*v*) and for repeated batch 3 it was 60% (*v*/*v*) (*n* = 1).

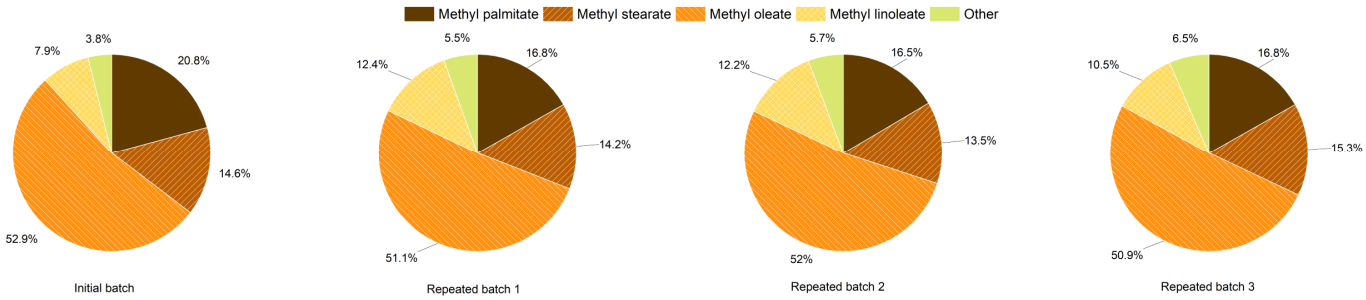

Figure 8. Fatty acid profile of the biomass of the endpoint of the 19 L transition-scale fermentations with *C. oleaginosum*. CG 1 was used for the initial batch and repeated batch 1, and CG 2 was used for repeated batch 2 and repeated batch 3. Inoculum for initial fermentation was 1% (*v*/*v*), for repeated batch 1 and 2 it was 5% (*v*/*v*) and for repeated batch 3 it was 60% (*v*/*v*) (*n* = 1).

In summary, the present results align well with and extend the existing literature in several important aspects. First, they reinforce the notion that untreated CG can be exploited as the sole carbon source for microbial lipid production by oleaginous yeasts, including *C. oleaginosum*, provided that appropriate feeding strategies are employed to mitigate inhibitory effects during early growth phases [23,34]. Second, they demonstrate that simple but effective process levers like staged feeding retain their effectiveness at the transition scale, which is fully consistent with previous reports on oxygen-managed, high-cell-density lipid fermentations [37,38]. Third, the maintenance of an oleate-dominated FA profile under CG feeding conditions highlights the robustness of lipid quality, an essential prerequisite for downstream biodiesel and oleochemical applications, and agrees with the generally reported FA patterns of yeast-derived SCO produced from glycerol [35].

4. Conclusions

This work closes an implementation gap between crude-glycerol feasibility studies and industrially relevant operation by demonstrating scalable, feeding-based inhibition control for *C. oleaginosum* on untreated, non-sterilized industrial CG. A single initial CG bolus caused complete growth arrest, underscoring that impurity-driven inhibition can dominate early cultivation phases. In contrast, distributing the same total crude-glycerol input via staged pulses restored respiratory activity, biomass formation, and lipid accumulation at 2.5 L and enabled robust transition-scale (19 L) repeated-batch fermentation for >640 h. Despite strong substrate-batch variability and increasing nitrogen limitation, the process maintained stable lipid levels (~30–36% CDW) and a consistent oleate-dominated fatty acid profile (~51–55% C18:1), indicating that lipid quality is resilient once inhibition is controlled.

Collectively, the findings support a clear practical message: robust lipid production from CG does not require detoxification if feeding is designed to minimize the inhibitor-to-biomass ratio during early growth, enabling reliable valorization of industrial-grade side streams.

5. Outlook and Recommendations

Future work may leverage inline surrogate measurements (such as conductivity or alkalinity) to anticipate inhibitor loads and adapt feeding in real time, as suggested by reviews of crude-glycerol impurity profiles and upgrading routes. Low-rate, feedback-controlled feeding tied to respiratory indicators (OTR/CTR) may further smooth inhibitor exposure beyond the simple staged schedule used here. Semi-continuous or cell-recycle strategies, which have been shown to support very high cell densities in oleaginous yeast processes, could be combined with the present approach to enhance productivity while retaining quality. Finally, a systematic exploration of inoculum size, ionic impurity load, and C/N interactions would more precisely map the operational window for untreated CG and enable predictive control strategies for industrial implementation.

Supplementary Materials: The following supporting information can be downloaded at: https://www.mdpi.com/article/10.3390/fermentation12030154/s1, Table S1: Composition of the lipid profiles of the stir tank fermentations; Table S2: Composition of the lipid profiles of the pilot scale fermentations.

Author Contributions: K.E.S., K.O. and A.N. conceived and designed the research. K.E.S. conducted experiments and wrote the manuscript. P.H., B.D. and M.S. conducted experiments. K.E.S. and A.N. supervised the experiments. K.E.S. analyzed data. K.E.S., K.O. and A.N. revised the manuscript. All authors have read and agreed to the published version of the manuscript.

Funding: Kevin E. Schulz and this work was funded by the project, FKZ 2220NR099B ELEGANT (Elektroimpulsbehandlung von Hefen zum Upcycling agroindustrieller Reststoffe zu Bioschmierstoffen und Einzellerproteinen.) from the German Bundesministerium für Ernährung und Landwirtschaft.

Institutional Review Board Statement: Not applicable.

Informed Consent Statement: Not applicable.

Data Availability Statement: The original contributions presented in this study are included in the article/Supplementary Material. Further inquiries can be directed to the corresponding authors.

Conflicts of Interest: The authors declare no conflicts of interest.

References

1. Ratledge, C. Fatty acid biosynthesis in microorganisms being used for Single Cell Oil production. *Biochimie* **2004**, *86*, 807–815. [CrossRef] [PubMed]
2. Ratledge, C.; Cohen, Z. Microbial and algal oils: Do they have a future for biodiesel or as commodity oils? *Lipid Technol.* **2008**, *20*, 155–160. [CrossRef]
3. Ratledge, C.; Wynn, J.P. The biochemistry and molecular biology of lipid accumulation in oleaginous microorganisms. *Adv. Appl. Microbiol.* **2002**, *51*, 1–51. [CrossRef]
4. Masri, M.A.; Garbe, D.; Mehlmer, N.; Brück, T.B. A sustainable, high-performance process for the economic production of waste-free microbial oils that can replace plant-based equivalents. *Energy Environ. Sci.* **2019**, *12*, 2717–2732. [CrossRef]
5. Dujon, B.A.; Louis, E.J. Genome Diversity and Evolution in the Budding Yeasts (Saccharomycotina). *Genetics* **2017**, *206*, 717–750. [CrossRef]
6. Bracharz, F.; Beukhout, T.; Mehlmer, N.; Bruck, T. Opportunities and challenges in the development of *Cutaneotrichosporon oleaginosus* ATCC 20509 as a new cell factory for custom tailored microbial oils. *Microb. Cell Fact.* **2017**, *16*, 178. [CrossRef]
7. Duman-Özdamar, Z.E. Engineering Oleaginous Yeasts for a Bio-Based Future. Ph.D. Thesis, Wageningen University, Wageningen, The Netherlands, 2025. [CrossRef]
8. Meesters, P.A.E.P.; Huijberts, G.N.M.; Eggink, G. High-cell-density cultivation of the lipid accumulating yeast *Cryptococcus curvatus* using glycerol as a carbon source. *Appl. Microbiol. Biotechnol.* **1996**, *45*, 575–579. [CrossRef]

9. Mhlongo, S.I.; Ezeokoli, O.T.; Roopnarain, A.; Ndaba, B.; Sekoai, P.T.; Habimana, O.; Pohl, C.H. The Potential of Single-Cell Oils Derived from Filamentous Fungi as Alternative Feedstock Sources for Biodiesel Production. *Front. Microbiol.* **2021**, *12*, 637381. [CrossRef] [PubMed]
10. Uğur, Ş.; Zieniuk, B.; Fabiszewska, A. Nutritional and Medicinal Properties of Microbial Oil. *Appl. Sci.* **2024**, *14*, 4232. [CrossRef]
11. Chilakamarry, C.R.; Sakinah, A.M.M.; Zularisam, A.W.; Pandey, A. Glycerol waste to value added products and its potential applications. *Syst. Microbiol. Biomanuf.* **2021**, *1*, 378–396. [CrossRef]
12. Awogbemi, O.; Desai, D.A. Recent advances in purification technologies for biodiesel-derived crude glycerol. *Int. J. Ambient Energy* **2025**, *46*, 2533373. [CrossRef]
13. Abdul Raman, A.A.; Tan, H.W.; Buthiyappan, A. Two-Step Purification of Glycerol as a Value Added by Product from the Biodiesel Production Process. *Front. Chem.* **2019**, *7*, 774. [CrossRef] [PubMed]
14. Liu, Y.; Zhong, B.; Lawal, A. Recovery and utilization of crude glycerol, a biodiesel byproduct. *RSC Adv.* **2022**, *12*, 27997–28008. [CrossRef]
15. Elgharbawy, A.S.; Sadik, W.A.; Sadek, O.M.; Kasaby, M.A. A Review on Biodiesel Feedstocks and Production Technologies. *J. Chil. Chem. Soc.* **2021**, *66*, 5098–5109. [CrossRef]
16. European Biodiesel Board (EBB). *EBB Statistical Report 2023*; European Biodiesel Board (EBB): Brussels, Belgium, 2023. Available online: https://ebb-eu.org/wp-content/uploads/2024/03/EBB_Statistical_Report2023-Final.pdf (accessed on 5 January 2026).
17. Almeida, E.L.; Olivo, J.E.; Andrade, C.M.G. Production of Biofuels from Glycerol from the Biodiesel Production Process—A Brief Review. *Fermentation* **2023**, *9*, 869. [CrossRef]
18. Johnson, D.T.; Taconi, K.A. The glycerin glut: Options for the value-added conversion of crude glycerol resulting from biodiesel production. *Environ. Prog.* **2007**, *26*, 338–348. [CrossRef]
19. Yu, Z.; Chang, Z.; Lu, Y.; Xiao, H. Metabolic engineering of *Saccharomyces cerevisiae* for glycerol utilization. *FEMS Yeast Res.* **2023**, *23*, foad014. [CrossRef]
20. Klein, M.; Swinnen, S.; Thevelein, J.M.; Nevoigt, E. Glycerol metabolism and transport in yeast and fungi: Established knowledge and ambiguities. *Environ. Microbiol.* **2017**, *19*, 878–893. [CrossRef]
21. Maza, D.D.; Barros, J.M.; Guillamón, J.M.; Aybar, M.J.; Viñarta, S.C. Valorization of Sugarcane Vinasse and Crude Glycerol for Single-Cell Oils Production by Rhodotorula glutinis R4: A Preliminary Approach to the Integration of Biofuels Industries for Sustainable Biodiesel Feedstock. *Fermentation* **2024**, *10*, 178. [CrossRef]
22. Ram, S.K.; Tyagi, R.D.; Drogui, P. Effect of Sludge Concentration and Crude Glycerol Matrix as a Substrate on the Production of Single-Cell Oil by Oleaginous Yeast *Yarrowia lipolytica SKY7*. *Fermentation* **2018**, *4*, 24. [CrossRef]
23. Signori, L.; Ami, D.; Posteri, R.; Giuzzi, A.; Mereghetti, P.; Porro, D.; Branduardi, P. Assessing an effective feeding strategy to optimize crude glycerol utilization as sustainable carbon source for lipid accumulation in oleaginous yeasts. *Microb. Cell Fact.* **2016**, *15*, 75. [CrossRef]
24. Poontawee, R.; Limtong, S. Feeding Strategies of Two-Stage Fed-Batch Cultivation Processes for Microbial Lipid Production from Sugarcane Top Hydrolysate and Crude Glycerol by the Oleaginous Red Yeast *Rhodosporidiobolus fluvialis*. *Microorganisms* **2020**, *8*, 151. [CrossRef]
25. Karamerou, E.E.; Theodoropoulos, C.; Webb, C. Evaluating feeding strategies for microbial oil production from glycerol by Rhodotorula glutinis. *Eng. Life Sci.* **2017**, *17*, 314–324. [CrossRef] [PubMed]
26. Gorte, O.; Kugel, M.; Ochsenreither, K. Optimization of carbon source efficiency for lipid production with the oleaginous yeast *Saitozyma podzolica* DSM 27192 applying automated continuous feeding. *Biotechnol. Biofuels* **2020**, *13*, 181. [CrossRef] [PubMed]
27. Lowry, O.; Rosebrough, N.; Farr, A.L.; Randall, R. Protein Measurement with the Folin Phenol Reagent. *J. Biol. Chem.* **1951**, *193*, 265–275. [CrossRef] [PubMed]
28. Yemm, E.W.; Willis, A.J. The estimation of carbohydrates in plant extracts by anthrone. *Biochem. J.* **1954**, *57*, 508–514. [CrossRef]
29. Hidalgo, P.; Toro, C.; Ciudad, G.; Navia, R. Advances in direct transesterification of microalgal biomass for biodiesel production. *Rev. Environ. Sci. Bio/Technol.* **2013**, *12*, 179–199. [CrossRef]
30. Solórzano, L. Determination of Ammonia in Natural Waters by the Phenolhypochlorite Method 1 1 This research was fully supported by U.S. Atomic Energy Commission Contract No. ATS (11-1) GEN 10, P.A. 20. *Limnol. Oceanogr.* **2003**, *14*, 799–801. [CrossRef]
31. Hartmann, L.; Martin, M.C.; Neumann, A.; Holtmann, D.; Ochsenreither, K. Understanding the Role of pH Regulation and Neutralizing Agents in Organic Acid Production and Growth of *Aspergillus oryzae*. *Biotechnol. Bioeng.* **2025**, *123*, 116–133. [CrossRef]
32. Kumar, L.R.; Yellapu, S.K.; Yan, S.; Tyagi, R.D.; Drogui, P. Elucidating the effect of impurities present in different crude glycerol sources on lipid and citric acid production by *Yarrowia lipolytica* SKY7. *J. Chem. Technol. Biotechnol.* **2020**, *96*, 227–240. [CrossRef]
33. Agyeman-Duah, E.; Kumar, S.; Gangwar, B.; Ujor, V.C. Glycerol Utilization as a Sole Carbon Source Disrupts the Membrane Architecture and Solventogenesis in *Clostridium beijerinckii* NCIMB 8052. *Fermentation* **2022**, *8*, 339. [CrossRef]

34. Pham, N.; Reijnders, M.; Suarez-Diez, M.; Nijsse, B.; Springer, J.; Eggink, G.; Schaap, P.J. Genome-scale metabolic modeling underscores the potential of *Cutaneotrichosporon oleaginosus* ATCC 20509 as a cell factory for biofuel production. *Biotechnol. Biofuels* **2021**, *14*, 2. [CrossRef]
35. Sara, M.; Brar, S.K.; Blais, J.F. Lipid production by *Yarrowia lipolytica* grown on biodiesel-derived crude glycerol: Optimization of growth parameters and their effects on the fermentation efficiency. *RSC Adv.* **2016**, *6*, 90547–90558. [CrossRef]
36. Duman-Ozdamar, Z.E.; Martins Dos Santos, V.A.P.; Hugenholtz, J.; Suarez-Diez, M. Tailoring and optimizing fatty acid production by oleaginous yeasts through the systematic exploration of their physiological fitness. *Microb. Cell Fact.* **2022**, *21*, 228. [CrossRef] [PubMed]
37. Chopra, J.; Sen, R. Process optimization involving critical evaluation of oxygen transfer, oxygen uptake and nitrogen limitation for enhanced biomass and lipid production by oleaginous yeast for biofuel application. *Bioprocess Biosyst. Eng.* **2018**, *41*, 1103–1113. [CrossRef]
38. Abeln, F.; Chuck, C.J. Achieving a high-density oleaginous yeast culture: Comparison of four processing strategies using *Metschnikowia pulcherrima*. *Biotechnol. Bioeng.* **2019**, *116*, 3200–3214. [CrossRef] [PubMed]